# Mechanisms of exchange bias in $DyFe_2/YFe_2$ exchange-coupled superlattices

M. R. Fitzsimmons
*Los Alamos National Laboratory, Los Alamos, New Mexico 87545, USA*

C. Dufour and K. Dumesnil
*Laboratoire de Physique des Matériaux, Université H. Poincaré, Nancy I, BP 239, 54506 Vandœuvre les Nancy Cedex, France*

Jian Dou and Michael Pechan
*Department of Physics, Miami University, Oxford, Ohio 45046, USA*

(Received 2 October 2008; revised manuscript received 28 January 2009; published 21 April 2009)

After cooling a $DyFe_2/YFe_2$ superlattice to 12 K in a 1 T field, which aligns the Fe spins parallel to the field, the magnetization vs field curve of the superlattice was dramatically shifted along the *magnetization and applied field axes*. The zero of the unpinned magnetization, i.e., the exchange bias, was −2 T. We developed a one-dimensional spin-chain model that completely explains the polarized neutron reflectometry, magnetometry, and x-ray magnetic circular dichroism data. Two domain configurations were identified in the model. Both configurations contribute to the extraordinarily large exchange bias of the $DyFe_2/YFe_2$ superlattice.

DOI: 10.1103/PhysRevB.79.144425 PACS number(s): 75.70.Cn, 75.30.Et, 61.05.fj

## I. INTRODUCTION

Traditionally, exchange bias is defined as the shift $H_E$ of the magnetization of a ferromagnet (FM) about the zero of applied field.[1,2] Exchange bias is often observed when unpinned spins of a FM are coupled to pinned spins of an antiferromagnet (AF) or a ferrimagnet.[3,4] In small applied fields, the coupling may cause the unpinned spins to point in a preferred direction—one possibly different from the applied field—producing a shift of the magnetization hysteresis loop along the applied field axis.

Exchange bias has important technological applications in "spin-valve" devices,[5] which are based on a switch fabricated from two FM layers—one pinned and the other unpinned. When the magnetic moment of the unpinned layer changes relative to the pinned layer, a change in resistance across the layers is produced. Exchange bias provides the force necessary to keep the reference magnetic layer pinned; thus, large exchange bias makes the magnetoresistance of spin valves robust.[6] In this paper we describe the origin of extraordinarily large exchange bias in the $DyFe_2/YFe_2$ superlattice.

Alternatively, a shifted magnetization loop can be observed in systems that are not saturated at both extremes of the field.[7] For example, if the magnitude of the field at which the loop closes for negative field is larger than that for positive field, then a minor (magnetization) loop is measured. A minor loop is shifted along the applied field axis for reasons unrelated to exchange anisotropy. Jacobs and Bean[7] noted that a shifted loop (arising from exchange bias) can be distinguished from a minor loop if the magnitudes of the magnetizations in the highest fields (positive and negative) are equal.

Since 1963, experimental tools have been developed, e.g., polarized neutron reflectometry (PNR) (Ref. 8) and x-ray magnetic circular dichroism (XMCD) (Ref. 9) that allow us to characterize magnetism in different components of a material. With these tools the magnetic response of unpinned magnetization can be distinguished from the pinned magnetization to determine whether a shift of the magnetization curve for the *unpinned* component is due to exchange anisotropy or to an artifact of the measurement (i.e., a minor loop). *These methods allow us to identify the reason for a shift that would otherwise be ambiguous.* The criterion for distinguishing between shifted and minor loops can be updated as follows: a shifted loop arising from exchange bias can be distinguished from a minor loop if the unpinned magnetizations in the highest fields (positive and negative) have equal magnitudes.

Most theories of exchange bias require uncompensated spins in the pinning layer, e.g., the AF or ferrimagnet that inhibits the response of a proximal FM through exchange coupling.[1,2,10–16] Pinned uncompensated magnetization has been reported in FM/AF bilayers such as $Fe/FeF_2$,[17] and $Fe/MnF_2$,[17] and $Co/Ni_{(1-x)}Fe_xF_2$ (Refs. 18 and 19) using superconducting quantum interference device (SQUID) magnetometry. In these systems, the direction of the pinned magnetization was (anti-)correlated with exchange bias. Pinned magnetization has been similarly inferred from shifts of the hysteresis loops along the magnetization axis for XMCD experiments in Co/NiO,[20] $Co/FeF_2$,[21] and Fe/MnPd (Ref. 22) bilayers. PNR has measured the thickness and magnitude of pinned magnetization in $Co/LaFeO_3$ (Ref. 23) and $Co/FeF_2$ (Refs. 24 and 25) bilayers. With the exception of $Co/Ni_{(1-x)}Fe_xF_2$ bilayers,[18,19] pinned magnetization of FM/AF systems is typically a percent or so of the saturation magnetization, and thus, challenging to detect and quantify. One motivation for studying the $DyFe_2/YFe_2$ model system is to understand the influence of pinned magnetization on exchange bias in a system in which the pinned magnetization is easy to quantify.

The response of unpinned magnetization to applied field, when the unpinned and pinned magnetizations are exchange coupled, may lead to an interface domain wall (iDW)—a domain wall parallel to the unpinned/pinned magnetization interface. iDWs in FM/AF bilayers (e.g., $Co/FeF_2$) have been inferred from magneto-optic Kerr effect (MOKE) spectroscopy[26] and PNR.[24] iDWs have also been found in

 

several rare-earth systems including FeSn/FeGd,[27] GdFe/TbFe,[28–30] $DyFe_2/YFe_2$,[31,32] TbFeCo/CoPd,[33] and SmCo/NdCo.[34]

$DyFe_2$ is a hard ferrimagnet with a net magnetization ($4.6\mu_B$/f.u. at 300 K) along the dominant Dy magnetization sublattice. $YFe_2$ is a soft ferrimagnet, but in contrast to $DyFe_2$, the Y site has only a small induced moment.[35] In $YFe_2$, the Fe contribution ($2.79\mu_B$/f.u. at 300 K) dominates. Due to the strong ferromagnetic exchange between Fe moments and the antiferromagnetic exchange between the larger Dy moment and smaller Fe moments, the magnetic coupling favors long-range antiparallel ordering of the $DyFe_2$ and $YFe_2$ magnetizations.

The rare-earth $Fe_2$ Laves phase superlattices are among the few single-crystalline systems[32,36,37] that exhibit spring magnet behavior.[38] Most of the other systems are either textured polycrystalline[39,40] or amorphous[29] materials, or consist of randomly oriented magnetically hard grains embedded in a soft matrix.[41–43] The $DyFe_2/YFe_2$ system exhibits a wide range of magnetization reversal processes, depending on the relative thicknesses of the two compounds: homogeneous reversal as a rigid magnetic block, inhomogeneous reversal in the soft component reminiscent of a spring magnet, or magnetization reversal beginning in the hard layers.[32] Recently, mixtures of these magnetization reversal mechanisms have been observed in other rare-earth iron systems.[44,45]

Exchange-coupled systems combining hard/soft ferromagnetic or ferrimagnetic materials offer opportunities to study specific issues pertaining to the pinning of the soft layer by the hard layer analogous to situations seen in FM/AF systems. In the case of $DyFe_2/YFe_2$, the hard layer ($DyFe_2$) can be relatively easily manipulated at room temperature by choosing the strength (typically a few tesla) and direction of the magnetic field to create a specific relationship between the magnetizations of the $DyFe_2$ and $YFe_2$ layers (for some FM/AF systems, the direction of the uncompensated pinned magnetization with respect to the cooling field is not known *a priori*). After cooling to low temperatures $DyFe_2$ becomes harder, and its orientation with respect to the cooling field can be very difficult to alter. Thus, by choosing the appropriate cooling field conditions, the magnetic domain state can be controlled to produce interesting magnetic phenomena such as exchange bias.

The aim of this study is to develop a microscopic understanding of the mechanisms leading to large exchange bias of the $DyFe_2/YFe_2$ superlattice. (The exchange bias is more than 1 order of magnitude larger than that found in FM/AF systems.) We developed a one-dimensional spin-chain model that self-consistently reproduces all the experimental data. The model suggests that the shift of magnetization along the field axis in our system might have two distinct origins corresponding to the behavior of two types of magnetic domains. For one type of domain, the magnetization reversed through nucleation of an iDW after application of a strong *negative* field (i.e., field opposite to the cooling field). For the second type of domain, an iDW was formed for small *positive* fields. After formation of an iDW, the magnetization rotated slowly and became fully reversed only for several tesla strong negative fields. This behavior produced a sheared hysteresis loop with zeros of the magnetization occurring at large negative fields. Both domain types contributed to the negative shift of the magnetization along the applied field axis. The large pinned magnetization shifted the hysteresis toward negative magnetization which also affected the shift of the magnetization along the applied field axis. The trivial consequence of a shift along the magnetization axis of a sheared loop on exchange bias is often not appreciated.

## II. SAMPLE PREPARATION AND CHARACTERIZATION

Growth and structural characterization with x-ray reflectometry of the $[DyFe_2(3\ \text{nm})/YFe_2(12\ \text{nm})]_{22}$ Laves phase sample was described in Ref. 31. Briefly, a 50-nm-thick single crystal of (110) Nb was grown on a $(11\bar{2}0)$ sapphire substrate at 700 °C using molecular-beam epitaxy. Next, 22 single-crystalline bilayers beginning with $DyFe_2$ and followed by $YFe_2$ were deposited. The [110] axis of $DyFe_2$ (and $YFe_2$) is along the sample surface normal. The thicknesses of the $DyFe_2$ ($2.8\pm0.7$ nm) and $YFe_2$ ($11.8\pm1.2$ nm) layers and interfacial roughness [$1.1\pm0.2$ nm(rms)] were obtained with x-ray reflectometry.[31] The sample was capped with 30 nm of Nb.

To establish exchange bias the sample was magnetized in a field of $\mu_0 H=7$ T applied parallel to $[\bar{1}10]$ at room temperature. The field was reduced to $\mu_0 H_{FC}=1$ T, and the sample was cooled to 12 K. $H_{FC}$ was chosen to be just large enough to align the Fe spins, thus, favoring the antiparallel arrangement of magnetizations from the $DyFe_2$ (dominated by Dy) and $YFe_2$ (dominated by Fe) layers [Fig. 1(a) of Ref. 31].

After field cooling, magnetometry data were taken with a SQUID from +7 T to −7 T (blue symbols, Fig. 1) and then back to +7 T [red symbols, Fig. 1(a)]. Qualitatively, the magnetization curve for the superlattice sample is remarkably similar to that for an ideal exchange-anisotropy-displaced-loop from $Ni_3Mn$ [see Fig. 2(a) of Ref. 46]. The average of the coercive fields is the exchange bias $H_E=-15.0\pm0.1$ kOe for our sample. In addition to $H_E$, the magnetization was shifted along the magnetization axis by $M^P=-81$ emu/cm$^3$. (The sign of the applied field $H_A$ is positive if $H_A$ and $H_{FC}$ point in the same direction.) The field at which $M=M^P$ was $H_E^u=-20$ kOe. Twice the coercive field $H_C$ at $H_E^u$ is approximately 1.1 kOe. The coercive field is typical of many exchange bias systems and usually attributed to some response of spins in the AF as the FM magnetization follows the applied field.[3]

In Fig. 1(b), we show the ac susceptibility as a function of applied (dc) field measured using a Quantum Design Physical Property Measurement System (PPMS). The susceptibility was obtained by superimposing a time-dependent perturbation on the dc field with a frequency of 10 kHz and peak amplitude of 15 Oe. The ac field was applied parallel to the dc field; thus, the measured response from the sample is related to the transverse component of the sample magnetization perpendicular to the dc field. The susceptibility is the ratio of the peak amplitude of the time varying *magnetization* normalized to the volume of the $YFe_2$ ($8.6\times10^{-6}$ cm$^3$) in the sample. The transverse magnetization is largest at $H_E^u$.

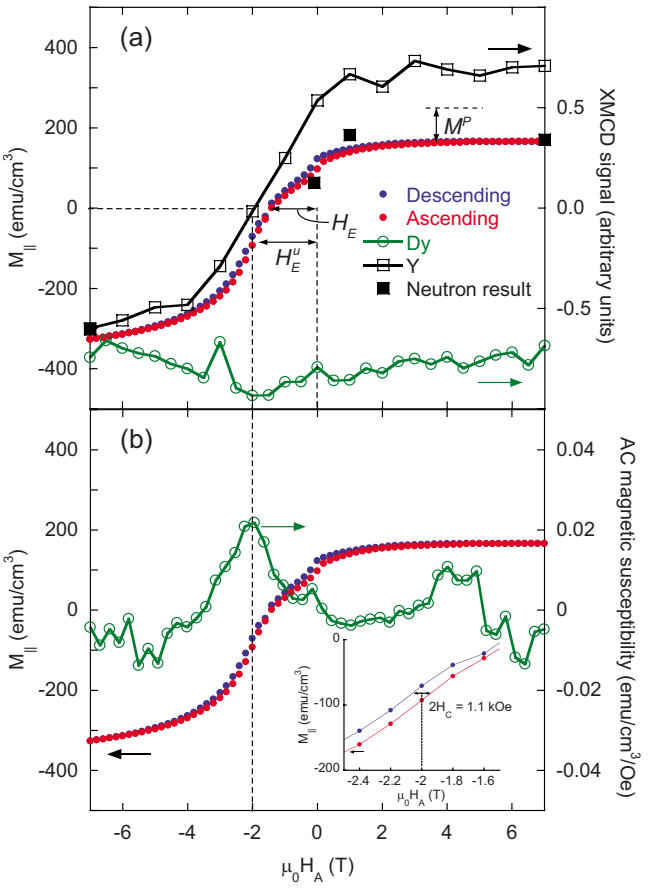


FIG. 1. (Color online) (a) Magnetization $M_{||}$ measured along the applied field $H_A$ (solid circles). XMCD taken at the absorption edges for Y (open squares) and Dy (open circles), and $M_{||}$ integrated over the magnetization depth profile obtained from neutron scattering (solid squares) are shown. (b) The susceptibility (green, open symbols) arising from the component of the magnetization that responds to an ac field perturbation added to the dc field $H_A$. Inset: expanded view showing the coercive field $H_C$ near $H_A = H_E^u$.

The XMCD fluorescence measured at the $L_3$ absorption edges of Dy and Y yielded the compound-selective hysteresis loops [Dy, green circles, and Y, open squares, Fig. 1(a)].[47] The induced moments on the Y site were less than 15% different for large $\pm|H_A|$. From these observations we conclude that the $YFe_2$ magnetization was unpinned. Zero Y moment coincides with $H_A = H_E^u$. We identify $H_E^u$ as the exchange bias of the unpinned magnetization. In contrast, the Dy moment exhibited little response to field; consequently, the $DyFe_2$ magnetization was pinned. The large negative moment of Dy suggests (and later confirmed with PNR) the pinned magnetization was opposite to $H_{FC} \| [\bar{1}10]$. This situation differs from our earlier study wherein $\mu_0 H_{FC} = 7$ T and $H_{FC} \| [\bar{1}10]$ resulted in the $DyFe_2$ magnetization being pinned mostly parallel to [001].[31] Thus, for small $H_{FC} \| [\bar{1}10]$, Fe spins on both sides of the $DyFe_2/YFe_2$ interface were parallel, which promoted exchange bias [see Eq. 7 in Ref. 3]. In contrast, for large $H_{FC} \| [\bar{1}10]$, Fe spins on either side of the interface were perpendicular, which suppressed exchange bias.[3]

## III. RESULTS FROM THE NEUTRON-SCATTERING EXPERIMENT

The field dependence of the magnetization depth profiles were obtained using PNR (Refs. 48–50) for fields of $\mu_0 H_A = +7$, $-7$, $-0.1$, and $+1$ T (in this order). The sample was field cooled as previously described. For a detailed discussion of the neutron-scattering experiment see Ref. 31. Briefly, the polarized neutron reflectivities were measured with two incident neutron beam polarizations called spin up, i.e., neutron spin parallel to $H_A$, and spin down (opposite to $H_A$). Since the direction of $H_A$ is fixed for our 11 T superconducting magnet, negative values of $H_A$ were achieved by reducing $H_A$ to zero, rotating the sample 180° about its surface normal *in situ*, and then increasing $H_A$ to the desired value.

The instrumental background corresponding to a reflectivity of order $10^{-7}$ was removed from the data. The diffuse scattering at the specular condition (where the angles of incidence and reflection were equal) was estimated from the off-specular scattering and removed to yield the specular reflectivity as a function of wave vector transfer $Q$. ($Q$ is the difference between the outgoing and incident neutron wave vectors.)

The off-specular scattering was weak at 12 K. The scattering was characterized by (Bragg) sheets of intensity that exhibited no variation with the component of $Q$ parallel to the sample surface $Q_{||}$ but was sharply peaked with the component of $Q$ perpendicular to the sample surface $Q_\perp$ corresponding to a superlattice Bragg reflection. The spin dependence of the off-specular scattering mirrored that of the Bragg reflections. Measurements of the off-specular x-ray scattering also found Bragg sheets with little or no variation in this intensity as a function of $Q_{||}$ over large regions of reciprocal space. We conclude that the weak off-specular neutron scattering is a consequence of the chemically rough (or stepped) $DyFe_2/YFe_2$ interfaces (see Fig. 2 of Ref. 31) transcending all lateral length scales.

The specular reflectivity normalized to the Fresnel reflectivity $R^F = 16\pi^2/Q^4$ is shown in Fig. 2. The data have been corrected for the nonperfect polarization of the neutron beam (polarization ~92%), the flipping efficiency of the neutron spin flipper (~99.9% efficient),[50,51] and the wavelength dependence of the neutron spectrum. The magnetization depth profiles were obtained for each field from an analysis of the dependence of the specular reflectivity on neutron polarization and $Q$. The solid curves in Fig. 2 are the reflectivities calculated from the magnetic structures shown in Fig. 3 (discussed later) that yielded the best fit, i.e., smallest value of $\chi^2$.[52]

We did not observe scattering that flipped the polarization of the neutron beam, i.e., so-called spin-flip scattering in this experiment. Previously, for experiments carried out under different conditions, spin-flip scattering was observed.[31] The conditions of the experiments differed in two ways. First, for the experiment in which spin-flip scattering was observed,[31] the sample was magnetized by a large field at room temperature, which induced a domain state with the $DyFe_2$ magnetization rotated away from the applied field that was subsequently frozen in place after cooling. Second, in the earlier

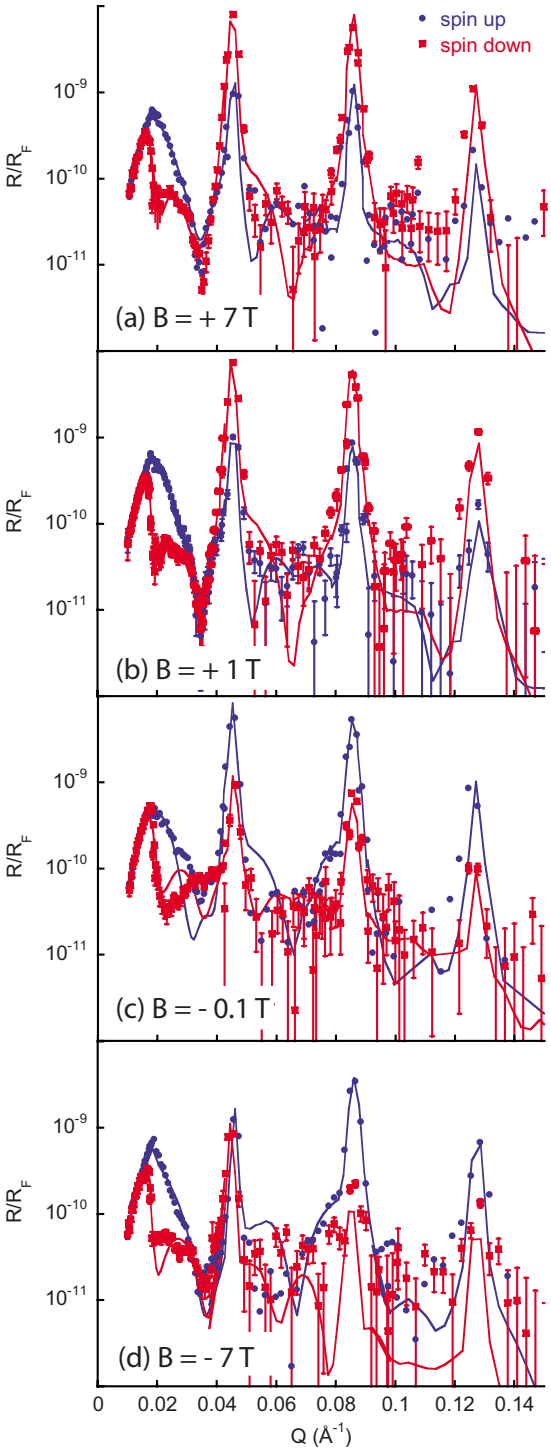


FIG. 2. (Color online) Field and neutron spin dependence of the reflectivities (symbols) normalized to the Fresnel reflectivity are shown. The curves are the reflectivities calculated from a neutron-scattering model (Fig. 3).

experiment,[31] field reversal (from +7 to −7 T) was achieved by rotating the sample in the 7 T field. (Magnetization reversal by rotation in a large field may induce coherent rotation of the magnetization in the same direction.) In the present experiment, the field was applied parallel (or antiparallel) to $[\bar{1}10]$ and *swept* from positive to negative values (relative to $[\bar{1}10]$) *through zero field*.

## IV. DISCUSSION

### A. Magnetometry data

The magnetometry data in Fig. 1 are notable because (1) the zero of magnetization occurs at a large negative field of the order of tens of kOe (i.e., the magnetization is shifted along the applied field axis), (2) the magnitudes of the most positive and negative magnetizations differ by 44% compared to their sum (i.e., the magnetization curve is shifted along the magnetization axis), (3) the ac susceptibility is maximum for $H_A = H_E^u$, and (4) magnetization reversal begins for small positive fields. The shift along the magnetization axis is due to the pinned magnetization of the $DyFe_2$ ferrimagnet, as made evident by the near-constant value of the XMCD signal for the Dy moment (Fig. 1). The reductions in the XMCD signal for the induced Y moment at remanence and the remanent magnetization are equal to ~75% of their saturation values, which indicate magnetization reversal begins for positive fields. This suggests that the easy axis of the unpinned magnetization is not parallel to $H_{FC} \| [\bar{1}10]$. In fact, had these measurements been obtained from a thin film rather than a superlattice, one would conclude that the easy axis of $YFe_2$ was rotated from $[\bar{1}10]$ by the angle $\varepsilon_{YFe_2} \sim \pi/4$. (The neutron-scattering observations of Ref. 31 suggest the unpinned magnetization rotates in the sample plane, so the easy axis is in the sample plane.) However, to account for the measured remanent magnetization of the superlattice, a portion of the $YFe_2$ layer must rotate by more than $\pi/4$, since other portions of the $YFe_2$ layer will be exchange coupled to the pinned magnetization (and thus less likely to rotate). The experimental data and results from a micromagnetic calculation (discussed later) agree best for $\varepsilon_{YFe_2} \sim \pi/2$ (e.g., the easy axis of $YFe_2$ in the superlattice is parallel to [001]).

### B. Neutron-scattering data

The neutron data show large differences between neutron spin-up and spin-down reflectivities just beyond the sample critical edge $Q_c \sim 0.017$ Å$^{-1}$ and for 3 orders of superlattice Bragg reflections $Q_1 = 0.045$, $Q_2 = 0.089$, and $Q_3 = 0.127$ Å$^{-1}$. $Q_c$ is the smallest value of the wave vector transfer where the neutron wave function is not purely imaginary.[50] Modeling of the neutron-scattering data (discussed later) suggests that spin dependence of the reflectivity near $Q_c$ was primarily influenced by the magnetization of the uppermost $YFe_2$ layer which tended to be aligned with $H_A$.

The intensities and neutron spin dependence of the Bragg reflections are related to the depth dependence of chemical and magnetic scattering length densities, respectively, having the period of the superlattice. The intensities of the Bragg reflections for one neutron spin state are larger than those of the other spin state by the same amount (except for the data taken at $\mu_0 H_A = -7$ T). The qualitative implication of this observation is that the magnetizations, while different for the two components ($DyFe_2$ and $YFe_2$), are reasonably uniform

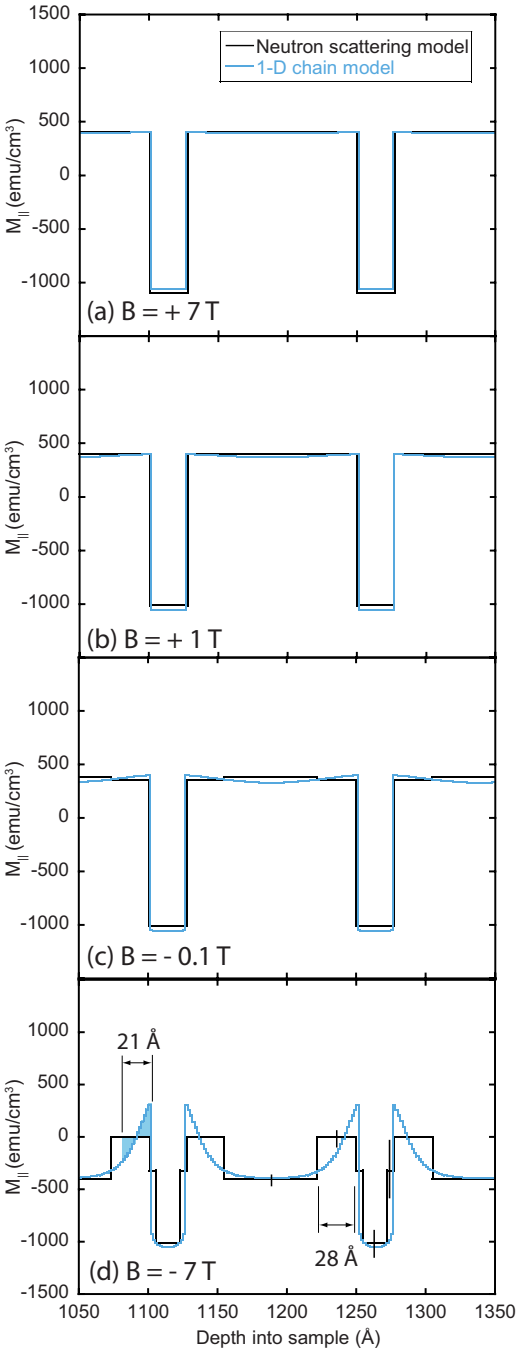


FIG. 3. (Color online) Magnetization depth profiles inferred from neutron scattering (black curves) and the one-dimensional chain model (light-colored curve) are shown. The error bars in (d) represent perturbations to the magnetization depth profile that increase the reduced (normalized) $\chi^2$ metric by 1.

in each layer for $\mu_0 H_A \geq -0.1$ T. On the other hand, for the case of $\mu_0 H_A = -7$ T, the spin-up and spin-down Bragg reflection intensities are the same for the first-order reflection ($Q = Q_1$), very different for the second-order reflection ($Q = Q_2$), and somewhat different for the third-order reflection ($Q = Q_3$). This variation is qualitatively explained by a nonuniform distribution of magnetization across the $DyFe_2/YFe_2$ bilayer that is repeated with the period of the superlattice.[53–55]

In order to understand the nature of the nonuniform magnetization, the data in Fig. 2 were quantitatively fitted to a neutron-scattering model. The neutron-scattering model consists of nuclear (chemical) and magnetic scattering length density depth profiles. The nuclear scattering length density was obtained from the chemical structure reported in Ref. 31. To represent a nonuniform distribution of magnetization across the periodically repeated $DyFe_2/YFe_2$ bilayer, we divided the magnetization of each $DyFe_2$ layer into three separate parts, and likewise for the $YFe_2$ layer. The magnetizations and thicknesses of the outer parts of each $DyFe_2$ layer were constrained to be the same. Similar constraints were applied to the $YFe_2$ layer. A portion of the magnetization depth profile for two periodically repeated $DyFe_2/YFe_2$ bilayers is shown in Fig. 3. The total magnetic layer thicknesses of the $DyFe_2$ and $YFe_2$ layers were constrained to be the same as their chemical thicknesses.

The spin-dependent neutron specular reflectivity was calculated using a variation in co-refine[50]—an implementation of the dynamical formulism of Parratt.[56] The process involved choosing six parameters for the neutron-scattering model from which the spin-dependent neutron-scattering length density depth profiles were calculated. The magnetizations of the $DyFe_2$ and $YFe_2$ layers were constrained to be less than their saturation magnetizations of $1055 \pm 45$ and $401 \pm 17$ emu/cm$^3$, respectively. The saturation magnetizations were obtained from analysis of PNR data taken from single-crystal films of each material at 7 T and 12 K (for $DyFe_2$) and 300 K (for $YFe_2$).[57] In addition to the six parameters that determine the periodic magnetic structure of the superlattice, the magnetizations of the uppermost $YFe_2$ and lowermost $DyFe_2$ layers were allowed to vary independently from the periodic bilayer. The two additional degrees of freedom are justified since the outermost layers were not pinned on both surfaces.[31]

Optimization of the parameters to minimize the $\chi^2$ metric[52] yielded the magnetization depth profile of the bilayer [a portion of the profile is shown in Fig. 3 (black curves)]. The total magnetization was obtained by integrating $M_{\|}$ over depth (Fig. 1, solid squares). The neutron-scattering result is in good quantitative agreement with magnetometry. Further, little change was observed in the magnetization of the $DyFe_2$ layers from neutron scattering, which confirms the conclusion that the $DyFe_2$ layers were pinned as obtained from the XMCD data.

The magnetization depth profiles for $\mu_0 H_A = -0.1$, +1, and +7 T are very similar, which is not surprising given the similarity of the Bragg reflections for these fields. [The neutron spin asymmetry of the Bragg reflections for data taken for $\mu_0 H_A = -0.1$ T was reversed compared to that for positive $H_A$ because the sample pinned magnetization was rotated (to gain access to $H_A < 0$), and neutron "spin up" and "spin down" are defined with respect to $H_A$.] However, at $\mu_0 H_A = -7$ T, the magnetization $M_{\|}$ of regions near the $DyFe_2/YFe_2$ interface was suppressed. The thicknesses of these regions were $28 \pm 2$ Å on the $YFe_2$ side of the $DyFe_2/YFe_2$ interface and $5 \pm 2$ Å on the $DyFe_2$ side.

Suppression of $M_{\|}$ at high negative field is consistent with an iDW, since the rotation of the magnetization away from the applied field increases the component of the magnetiza-

TABLE I. Values of the parameters used in the one-dimensional chain model to represent the magnetization of the $DyFe_2/YFe_2$ superlattice at 12 K (after field cooling from room temperature in $\mu_0 H_{FC}=1$ T). The value used for the exchange across the $DyFe_2/YFe_2$ interface $A_{int}$ is the same as the exchange in the constituent layers, i.e., $A_{Fe\text{-}Fe}$.

| | $DyFe_2$ | $YFe_2$ | Note |
|---|---|---|---|
| $M_s$(emu/cm$^3$) | $1055 \pm 45$ | $401 \pm 17$ | Analysis of PNR data from single-crystal thin films (this work). |
| $K$(erg/cm$^3$) | $(1.2 \pm 0.7) \times 10^8$ | $1.3 \times 10^6$ (Ref. 67) | Reference 31 for 250 K |
| $A_{Fe\text{-}Fe}$(erg/cm) | $2 \times 10^{-6}$ | $2 \times 10^{-6}$ | Reference 68 |
| $\varepsilon$ (rad) | 0 (easy axis$\parallel[\bar{1}10]$) | $\pi/2$ (easy axis$\parallel$[001]) | $\varepsilon_{DyFe_2}=0$ was obtained from analysis of PNR and XMCD data (this work). $\varepsilon_{YFe_2}=\pi/2$ yielded the calculated result. |
| $\theta$ (rad) | $\pi$ | 0 | Orientation of the layer magnetization with respect to the Fe spin. |

tion perpendicular to the applied field $M_\perp$ [as suggested by the ac susceptibility data in Fig. 1(b)] at the expense of $M_\parallel$. The specular reflectivity is sensitive to the sample magnetization averaged over the lateral coherence of the neutron beam (tens of microns).[58] Therefore, we expect an iDW with large lateral area to produce spin-flip specular reflectivity $R^{SF}$, since $R^{SF} \propto \langle M_\perp^2 \rangle$ for large domains, provided that $M_\perp$ is perpendicular to $Q$. However, $R^{SF}$ was not observed after the field was swept from positive to negative values through zero field, so we conclude that if iDWs were present, $M_\perp$ averaged over the lateral coherence of the neutron beam was too small to detect, and/or $M_\perp$ was parallel to $Q$.

Off-specular scattering may contain information about $M_\perp$ for small domains, provided that the scattering is strong enough to detect, $M_\perp$ is perpendicular to $Q$, and the scattering from the domains is accessible to off-specular neutron reflectometry. The region of reciprocal space accessible to off-specular neutron reflectometry corresponds to $Q_\parallel$ less than $\sim 10^{-4}$ Å$^{-1}$. This length scale is sensitive to domains with lateral size of order 1 $\mu$m. The off-specular scattering was weak at 12 K and consistent with the chemical roughness of the interfaces; thus, we lack evidence for scattering from micron-sized domains in these data.

### C. Comparison of exchange bias of the $DyFe_2/YFe_2$ superlattice with other systems

The interface energy density[12] $\Delta E = H_E^u 2 t_{FM} M_{FM} = 10.6$ erg/cm$^2$ is a measure of the strength of exchange coupling across the $YFe_2/DyFe_2$ interface. To evaluate $\Delta E$ $M_{FM}=M_{YFe_2}=401$ emu/cm$^3$ (obtained from neutron scattering) and $t_{FM}=t_{YFe_2}/2=60$ Å were used (the factor of $\frac{1}{2}$ is required since an $YFe_2$ layer is bounded on both sides by $DyFe_2$ layers). The interface energy density for the $YFe_2/DyFe_2$ interface is very large—1 order of magnitude larger than those of FM/AF bilayers and comparable to that of TbFeCo ferrimagnet/ferrimagnet bilayers.[59]

Recently, Fitzsimmons *et al.*[25] concluded from a study of the $Co/FeF_2$ system that exchange bias was most likely related to the areal pinned moment density (the integral of the pinned interfacial magnetization over its depth). For the $Co/FeF_2$ sample, $\Delta E = 3$ erg/cm$^2$ and the areal pinned moment density was $\sim(1.4 \pm 0.2) \times 10^{-5}$ emu/cm$^2$.[25] Comparing to the $DyFe_2/YFe_2$ system, the ratios of $\Delta E_{YFe_2/DyFe_2}/\Delta E_{Co/FeF_2} \approx 3.5$ and areal pinned moment density of $DyFe_2/YFe_2$ to $Co/FeF_2$ $1.5 \times 10^{-4}/1.4 \times 10^{-5} \approx 11$, differ by a factor of about 3. If in general, the areal pinned moment density controls the magnitude of $H_E$, then only pinned spins within $\sim 10$ Å of the interface would play a direct role in establishing exchange bias in $DyFe_2/YFe_2$ (although spins further from the interface may serve as an anchor for anisotropy of the interface[59]).

Mangin *et al.*[29] used a simple formulism for the free energy of a compressed domain wall to explain their magnetometry observations for GdFe/TbFe/GdFe trilayers. Following their approach and using reasonable values for the Fe-exchange $A_{Fe\text{-}Fe}$, anisotropy of $YFe_2$, $K_{YFe_2}$, and anisotropy of $DyFe_2$, $K_{DyFe_2}$(Table I), we calculated Fe-spin rotations $\phi$ of $86° \pm 9°$ and $33° \pm 19°$ on the $YFe_2$ and $DyFe_2$ sides of the $DyFe_2/YFe_2$ interface, respectively. These values were obtained for $\mu_0 H_A = -7$ T using $\delta = \phi \sqrt{A/K + 2M_s/|H_A|}$ where $\delta_{YFe_2}=28$ Å and $\delta_{DyFe_2}=5$ Å [Fig. 3(d)]. The sum of the rotation angles underestimates a $\pi$ rotation of Fe spins across the iDW by one third. The discrepancy may be due to the fact that the condition $t_{FM} \gg \delta$ for the expression of $\delta$ is not satisfied for our system.

Morales *et al.*[60] observed a strong dependence of exchange bias in FM/AF/FM trilayers with the relative magnetic state of the two FMs during field cooling, thus, implying a strong coupling (interaction) *across a thick AF* (in this instance $FeF_2$). For our sample, the thickness of the $DyFe_2$ layer is only one tenth that of the AF layer studied by Morales *et al.*;[60] therefore, adjacent $DyFe_2/YFe_2$ layers may be coupled across the $DyFe_2$ layer. The magnetic behavior might also be affected by the proximal location of $DyFe_2/YFe_2$ interfaces across a thin $YFe_2$ layer. For example, twice the iDW thickness for a $\pi$ rotation of Fe spins at $H_A=H_E$ is greater than the thickness of the $YFe_2$ layer ($\sim 144$ Å compared to 120 Å). These points argue for the possibility that the magnetism of adjacent interfaces affects

each other, and therefore, the formulism of Mangin *et al.*[29] may not be applicable to our case.

### D. Micromagnetic modeling with the spin-chain model and mechanisms of exchange bias

In view of this possibility, we calculated the magnetic depth profile and magnetization for a one-dimensional chain of spins. The superlattice was represented by a chain of 75 spins in the $YFe_2$ layer and 15 spins in the $DyFe_2$ layer (repeated 22 times). The spin configuration $\phi_i$, where $\phi_i$ is the orientation of the Fe spins in the $i$th layer, was optimized to minimize the free energy [Eq. (1)] for the values of $M_s$, $A$, $K$, $\varepsilon$, and $\theta$ given in Table I. The value used for the exchange across the $DyFe_2/YFe_2$ interface was $A_{\text{int}}=2\times10^{-6}$ erg/cm (the same value as used for the exchange between two Fe spins in the adjacent layers),

$$E=-\sum_{i=1}^{N-1}\frac{A_{i,i+1}}{d_{i,i+1}^2}\cos(\phi_{i+1}-\phi_i)+\sum_{i=1}^{N}K_i\sin^2(\phi_i-\varepsilon_i)$$
$$-H\sum_{i=1}^{N}M_i\cos(\phi_i+\theta_i). \quad (1)$$

$\theta$ is the orientation of the layer magnetization with respect to the Fe spin. $\varepsilon$ is the easy axis of the layer in the sample plane with respect to $[\bar{1}10]$ (the direction of positive applied field). Since the (110) planes of $DyFe_2$ and $YFe_2$ have hexagonal symmetry, uniaxial anisotropy leading to the $\sin^2$ dependence on $\phi$ is a reasonable choice in Eq. (1).[61,62] We found three equal low-energy configurations (domains), which in keeping with the notation used by previous authors,[44,45] are called $\sigma^+$, $\sigma^-$, and $\sigma^0$.

In the spin-chain model, magnetization reversal of $\sigma^{\pm}$ domains occurred via rotation of the $YFe_2$ magnetization starting near the center of the film for small positive fields, and then progressed toward the $DyFe_2/YFe_2$ interface with increasingly more negative fields [see insets of Fig. 4(a)]. The rotation may be positive ($\sigma^+$) or negative ($\sigma^-$) about the sample surface normal [see Figs. 4(b) and 4(c)]. In order to produce the rounding of the magnetization for $H_A>0$, the easy axis of $YFe_2$ must not be parallel to $[\bar{1}10]$, i.e., $\varepsilon_{YFe_2}\neq0$.[63]

We investigated the influence of $\varepsilon_{YFe_2}$ on the calculated magnetization curve and found best agreement with the experiment for $\varepsilon_{YFe_2}=\pi/2$ [black curve in Fig. 4(a)]. For comparison, the magnetization anticipated from an average of $\sigma^{\pm}$ and $\sigma^0$ domains for $\varepsilon_{YFe_2}=\pi/4$ is shown by the gray curve in Fig. 4(a). This choice yielded a curve that greatly overestimated the magnetization for $\mu_0H_A$ between −3 and −1 T compared to the data. In addition, smaller values of $\varepsilon_{YFe_2}$ predicted much larger exchange bias than was observed. This prediction suggests a means to increase exchange bias.

Previously, for SmCo/Fe bilayers, the Fe layer was observed to reorient from parallel to perpendicular with respect to the easy axis of the hard (SmCo) layer.[64] The reorientation was explained by partial remagnetization of the hard layer after field cycling that produced regions of different bilinear coupling (i.e., coupling that fluctuated from region to region). Averaging of the fluctuating magnetization led to biquadratic interlayer exchange coupling. [A similar mechanism was proposed for the appearance of the 45° exchange coupling in $Fe/FeF_2$ (twinned) bilayers.[65]] It is unclear whether fluctuating magnetization in the $DyFe_2$ layer plays a role in the appearance of an easy axis in the $YFe_2$ layer along its [001] direction. The x-ray and neutron data indicate that the $DyFe_2$ magnetization does not respond to field; however, the data would not likely be sensitive to the rotation of Dy moments in a single monolayer at the interface (such rotation might also give rise to the observed nonzero value of $H_C$).

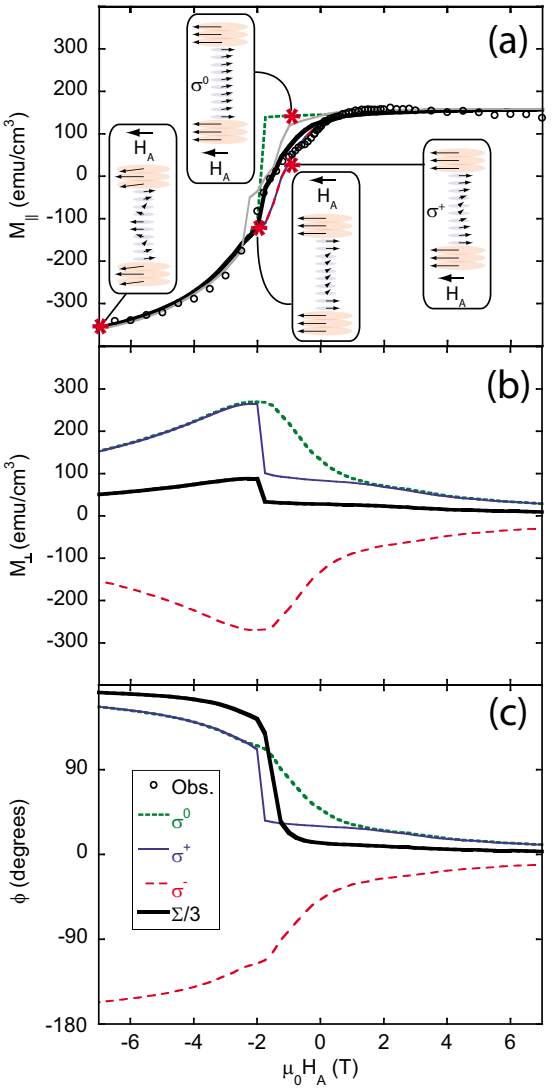


FIG. 4. (Color online) (a) The magnetization parallel to the applied field data from Fig. 1 (circles), calculated for the $\sigma^{\pm}$ domains (blue/red dashed curve), $\sigma^0$ domain (green dotted curve), and the average of the three domains $\Sigma/3$ (black curve) using $\varepsilon_{YFe_2}=\pi/2$ are shown. The average magnetization from the three domains is shown (gray curve) for $\varepsilon_{YFe_2}=\pi/4$. Inset: schematic of the configuration of moments in the $YFe_2$ layer surrounded by $DyFe_2$ moments for fields marked by "*". (b) The magnetization perpendicular to the applied field. (c) The angle $\phi$ between the calculated magnetizations for each domain in the sample plane with respect to $H_{FC}\|[\bar{1}10]$.

For $\sigma^{\pm}$ domains and small enough positive fields, the magnetic free energy was minimized when many of the $YFe_2$ moments rotated away from the applied field toward the $YFe_2$ easy axis. As the field became negative, minimization of the Zeeman energy was the driving force that caused the moments to rotate beyond the easy axis toward the field direction. [Experimental evidence supporting rotation of the magnetization from the applied field is the ac susceptibility measurement in Fig. 1(b).] Consequently, the field dependence of $M_{\|}$ due to compression of an iDW was sheared (or rounded) as a function of field. Since the magnetization varied slowly over a few tesla for our system, the shift of the magnetization along the applied field axis was partially dependent on the large pinned $DyFe_2$ magnetization. Magnetization reversal of $\sigma^{\pm}$ domains yielded a shift of the magnetization along the applied field axis that was ~3 kOe too small [see blue and red curves Fig. 4(a)] compared to the data.

The exchange bias we infer for the $\sigma^{\pm}$ domains from our spin-chain model can be compared to literature reports for exchange bias in systems exhibiting similar magnetization reversal mechanisms. For example, the formation of the partial domain wall in SmCo/NdCo bilayers[34] and compression of the iDW giving rise to $\sigma^{\pm}$ domains in TbFe/GdFe bilayers[45] are the same. In the case of SmCo/NdCo, exchange bias was also observed[34] and treated using a variation in the model of Mauri *et al.*[15] for exchange bias. Rather than allowing for the formation of a domain wall in the hard (SmCo) layer—akin to the antiferromagnet in the model of Mauri *et al.*[15]—Guo *et al.*[34] considered the situation where the domain wall formed inside the soft (NdCo) ferromagnet (a key insight of the Kiwi[11] model for exchange bias). An expression for exchange bias relating it to properties intrinsic to the soft ferromagnet (anisotropy $K$, exchange $A$, and magnetization $M$) and its thickness $t$ was derived. Specifically, $H_E=-2\sqrt{KA}/Mt$. Using the values listed in Table I and identifying $t$ as one half the $YFe_2$ thickness (because this layer is bounded on both sides by pinning layers in our superlattice), we obtain $H_E=-13$ kOe. The agreement between this prediction and that (−12 kOe) calculated for the $\sigma^{\pm}$ domains of the spin-chain model is not surprising since both approaches represent the reversal of magnetization in the soft layer similarly, i.e., by compression of a planar domain wall in the soft layer. The predicted exchange bias was nevertheless smaller than observed; thus, compression of the iDW in $\sigma^{\pm}$ domains is not entirely responsible for exchange bias (in the $DyFe_2/YFe_2$ superlattice). In addition, the formulism of Guo *et al.*[34] does not account for the commensurate affect of a shift of a sheared hysteresis loop along its magnetization axis (due to pinned magnetization) on exchange bias.

An alternative method to achieve a minimum free energy involved rotation of the $YFe_2$ magnetization away from the applied field *uniformly* over the majority of the $YFe_2$ layer [inset of Fig. 4(a)]. This mechanism minimized the total energy by reducing the exchange and anisotropy energies at the expense of increased Zeeman energy for small positive fields. [The exception is for spins in close proximity to the $DyFe_2/YFe_2$ interface where the interfacial exchange tended to keep spins parallel to the applied field (reducing the Zeeman energy) at the expense of increased exchange energy from rotation of the Fe spins on the $YFe_2$ side of the interface in proximity to the interface.] For a large enough negative field, the Zeeman energy would exceed any gains that could be obtained by minimizing the exchange and anisotropy energies. For this field, the center portion of the soft magnetization flipped, thus, nucleating an iDW (at the $DyFe_2/YFe_2$ interface). As was the case for the $\sigma^{\pm}$ domains, minimization of the Zeeman energy was the driving force that compressed the iDW with increasingly more negative fields. The primary difference between the two domain types is that iDWs are formed in $\sigma^{\pm}$ domains with small positive fields, whereas modest negative fields are required to transform $\sigma^0$ domains into $\sigma^{\pm}$ domains. The change in energy of an iron moment that flips in a field of $H_E^u=-20$ kOe is about one half the thermal energy of the atom at 12 K. Magnetization reversal of $\sigma^0$ domains led to a shift of the magnetization along the applied field axis that was ~3 kOe too large [see green curve in Fig. 4(a)] compared to the data.

Previously, McCord *et al.*[45] directly observed coexistence of the three domain types ($\sigma^0$, $\sigma^+$, and $\sigma^-$) in TbFe/GdFe bilayer samples during magnetization reversal with Kerr microscopy. Direct observation of these domains using their technique is not possible in a superlattice.

One could ask whether the rotation of magnetization across a Néel domain wall—a domain wall that is perpendicular to the sample plane (as opposed to an iDW)—could be detected as off-specular neutron scattering. (The rotation of magnetization across a Bloch wall brings the magnetization parallel to $Q$, so PNR is not particularly sensitive to Bloch walls.) Using the values for the anisotropy and exchange given in Table I, the domain-wall widths for $DyFe_2$ and $YFe_2$ are at most ~4 and ~39 nm, respectively. The volume fraction of spins in a domain wall compared to a 1-$\mu$m-wide domain is less than 3%. About a third of these spins may produce spin-flip scattering. The contribution of these spins to the off-specular scattering would be challenging to detect from 1-$\mu$m-size domains. However, for 10-nm-size domains, the domain walls would contain a larger fraction of spins and might be more easily detected were it not for the difficulty that off-specular PNR does not have practical access to such small lateral features.[66]

Since the difference between the free energies for the $\sigma^{\pm}$ and $\sigma^0$ domains was not computationally significant (less than 1 part in 5000), we assumed that the three domains were equally populated. Thus, to compute the depth profile $M_{\|}$ of the chain model, the magnetization depth profiles from the three domains were averaged. The depth profile is shown by the light-colored curve in Fig. 3. To compare depth profiles of the chain and neutron-scattering models, we asked how thick would the interfacial region need to be in the chain model to have the same magnetization as that of the neutron-scattering model (for $\mu_0 H_A=-7$ T). The answer [shown by the shaded region in Fig. 3(d)] was 21 Å for the chain model, which is in good agreement with the 28 Å value for the neutron-scattering model.

We compared the calculated values for $M_{\|}(H_A)$ obtained by integrating the magnetization depth profile from the spin-chain model with the magnetometry data. (The average magnetization perpendicular to the applied field $M_{\perp}(H_A)$ was also calculated [Fig. 4(b)] and was small relative to $M_{\|}$ for

fields measured in the neutron experiment.) For $\varepsilon_{YFe_2}=\pi/2$ (*the only adjustable parameter in the chain model*), good agreement between the calculated and observed magnetization curves was obtained. Specifically, the rounded magnetization observed for $\mu_0 H_A \sim 0$ T was reproduced. The rounding of the magnetization near zero field was best accounted for by $\sigma^{\pm}$ domains in the chain model. However, these domains alone could not account for the shift of the magnetization along the applied field axis, which was better explained by a combination of $\sigma^0$ and $\sigma^{\pm}$ domains. The transverse magnetization from all three domains is maximum near $H_E$ [Fig. 4(b)] where the ac susceptibility is also maximum [Fig. 1(b)].

## V. CONCLUSIONS

In summary, after cooling the $DyFe_2/YFe_2$ superlattice to 12 K in a small field of 1 T, which was used to align the Fe spins parallel to the field during cooling, the field dependence of the magnetization was shifted dramatically along the *magnetization and applied field axes*. From the polarized neutron reflectivities, we obtained magnetization depth profiles for a few applied fields. At $\mu_0 H_A=-7$ T, the magnetization along the applied field was nearly zero in a region $\sim 28$ Å thick residing mostly in the $YFe_2$ layer close to the $DyFe_2/YFe_2$ interface. The magnetization of the $DyFe_2$ was mostly unchanged with field—a result consistent with observations from XMCD which suggest that the magnetization of the $DyFe_2$ was pinned. The magnetization integrated over the entire depth profile obtained from PNR is in good quantitative agreement with the magnetometry data.

The combination of probes with element (XMCD) or position (PNR) sensitivity to measure the response of magnetization of the constituents of a composite material allowed us to understand magnetization of the ensemble better than had we relied solely upon bulk probes. For example, the shift of the magnetization along the field axis is primarily the result of exchange bias of the unpinned $YFe_2$ magnetization and not the consequence of incomplete saturation of this magnetization (i.e., the shift is not an artifact of a minor loop reversal). The shift of the sheared magnetization curve along the magnetization axis (due to the pinned $DyFe_2$ moment) also affected $H_E$ to a lesser extent but in a manner that tended to reduce the magnitude of $H_E$.

We showed that application of simple analytical relations to calculate domain-wall widths does not work well for our superlattice system. This failure led us to develop a spin-chain model that reproduced the magnetization depth profiles inferred from neutron scattering using one adjustable parameter (the orientation of the $YFe_2$ easy axis). In addition, the magnetization calculated using the spin-chain model reproduced the shifts of the magnetization along the magnetization and applied field axes, the field dependence of the magnetization, and is consistent with the ac susceptibility data. The ac susceptibility data imply a maximum in the transverse magnetization at $H_E$. We found three energetically equivalent domains for the chain model. Magnetization reversal of the $\sigma^0$ domain was accomplished by coherent rotation of the soft layer magnetization by a small amount that was mostly uniform across its thickness, followed by nucleation of an iDW at the critical field $H_E^{\sigma^0}=-18$ kOe, and then compression of the iDW with more negative fields. In contrast, iDWs were formed for small positive fields in $\sigma^{\pm}$ domains with the domain wall transcending half the thickness of the soft layer, and then compressing for more negative fields. A −12 kOe shift of the magnetization curve along the field axis for the $\sigma^{\pm}$ domains is a consequence of a slowly varying field dependence of the magnetization combined with a shift along the magnetization axis by a source of pinned magnetization. The thickness of the iDW at $\mu_0 H_A=-7$ T calculated using the chain model is in close agreement with the thickness of the region of suppressed magnetization obtained from neutron scattering. The success of the spin-chain model in reproducing all the experimental data gives us confidence that the model can be used to reliably predict the magnetic behavior of other related systems.

## ACKNOWLEDGMENTS

We acknowledge valuable discussions with S. Mangin (Université Nancy). This work was supported by the Office of Basic Energy Science, U.S. Department of Energy, BES-DMS at LANSCE, and the Miami University. This work has benefited from the use of the Lujan Neutron Scattering Center at LANSCE, which is funded by the Office of Basic Energy Science, Department of Energy. Los Alamos National Laboratory is operated by Los Alamos National Security LLC under DOE (Contract No. DE-AC52-06NA25396). M.R.F. gratefully acknowledges financial assistance from the Université Nancy.

[1] W. H. Meiklejohn and C. P. Bean, Phys. Rev. **102**, 1413 (1956).
[2] W. H. Meiklejohn and C. P. Bean, Phys. Rev. **105**, 904 (1957).
[3] J. Nogués and I. K. Schuller, J. Magn. Magn. Mater. **192**, 203 (1999).
[4] A. E. Berkowitz and K. Takano, J. Magn. Magn. Mater. **200**, 552 (1999).
[5] B. Dieny, J. Magn. Magn. Mater. **136**, 335 (1994).
[6] I. R. McFadyen, E. E. Fullerton, and M. J. Carey, MRS Bull. **31**, 379 (2006).
[7] I. S. Jacobs and C. P. Bean, *Fine Particles, Thin Films, and Exchange Anisotropy in Magnetism*, edited by G. T. Rado and H. Suhl (Academic, New York, 1963), Vol. 3, Chap. 6, pp. 323–330; I. S. Jacobs and C. P. Bean, *Fine Particles, Thin Films, and Exchange Anisotropy in Magnetism*, edited by G. T. Rado and H. Suhl (Academic, New York, 1963), Vol. 3, Chap. 6, p. 324.
[8] M. R. Fitzsimmons, S. D. Bader, J. A. Borchers, G. P. Felcher, J.

K. Furdyna, A. Hoffmann, J. B. Kortright, Ivan K. Schuller, T. C. Schulthess, S. K. Sinha, M. F. Toney, D. Weller, and S. Wolf, J. Magn. Magn. Mater. **271**, 103 (2004).
[9] J. B. Kortright, D. D. Awschalom, J. Stöhr, S. D. Bader, Y. U. Idzerda, S. S. P. Parkin, I. K. Schuller, and H. C. Siegmann, J. Magn. Magn. Mater. **207**, 7 (1999).
[10] R. L. Stamps, J. Phys. D **33**, R247 (2000).
[11] M. Kiwi, J. Magn. Magn. Mater. **234**, 584 (2001).
[12] A. P. Malozemoff, Phys. Rev. B **35**, 3679 (1987).
[13] U. Nowak, K. D. Usadel, J. Keller, P. Miltényi, B. Beschoten, and G. Güntherodt, Phys. Rev. B **66**, 014430 (2002).
[14] J. Keller, P. Miltényi, B. Beschoten, G. Güntherodt, U. Nowak, and K. D. Usadel, Phys. Rev. B **66**, 014431 (2002).
[15] D. Mauri, H. C. Siegmann, and P. S. Bagus, J. Appl. Phys. **62**, 3047 (1987).
[16] T. C. Schulthess and W. H. Butler, Phys. Rev. Lett. **81**, 4516 (1998).
[17] J. Nogués, C. Leighton, and I. K. Schuller, Phys. Rev. B **61**, 1315 (2000).
[18] M. Cheon, Z. Liu, and D. Lederman, Appl. Phys. Lett. **90**, 012511 (2007).
[19] M. Cheon, L. Zhongyuan, and D. Lederman, J. Appl. Phys. **101**, 09E503 (2007).
[20] H. Ohldag, T. J. Regan, J. Stöhr, A. Scholl, F. Nolting, J. Lüning, C. Stamm, S. Anders, and R. L. White, Phys. Rev. Lett. **87**, 247201 (2001).
[21] H. Ohldag, H. Shi, E. Arenholz, J. Stöhr, and D. Lederman, Phys. Rev. Lett. **96**, 027203 (2006).
[22] S. Brück, G. Schütz, E. Goering, X. Ji, and K. M. Krishnan, Phys. Rev. Lett. **101**, 126402 (2008).
[23] A. Hoffmann, J. W. Seo, M. R. Fitzsimmons, H. Siegwart, J. Fompeyrine, J. P. Locquet, J. A. Dura, and C. F. Majkrzak, Phys. Rev. B **66**, 220406(R) (2002).
[24] S. Roy, M. R. Fitzsimmons, S. Park, M. Dorn, O. Petracic, I. V. Roshchin, Z.-P. Li, X. Batlle, R. Morales, A. Misra, X. Zhang, K. Chesnel, J. B. Kortright, S. K. Sinha, and I. K. Schuller, Phys. Rev. Lett. **95**, 047201 (2005).
[25] M. R. Fitzsimmons, B. J. Kirby, S. Roy, Z.-P. Li, I. V. Roshchin, S. K. Sinha, and I. K. Schuller, Phys. Rev. B **75**, 214412 (2007).
[26] I. V. Roshchin, O. Petracic, R. Morales, Z.-P. Li, X. Batlle, and I. K. Schuller, Europhys. Lett. **71**, 297 (2005).
[27] F. Canet, S. Mangin, C. Bellouard, and M. Piecuch, Europhys. Lett. **52**, 594 (2000).
[28] S. Mangin, F. Montaigne, and A. Schuhl, Phys. Rev. B **68**, 140404(R) (2003).
[29] S. Mangin, G. Marchal, and B. Barbara, Phys. Rev. Lett. **82**, 4336 (1999).
[30] Y. Henry, S. Mangin, T. Hauet, and F. Montaigne, Phys. Rev. B **73**, 134420 (2006).
[31] M. R. Fitzsimmons, S. Park, K. Dumesnil, C. Dufour, R. Pynn, J. A. Borchers, J. J. Rhyne, and Ph. Mangin, Phys. Rev. B **73**, 134413 (2006).
[32] K. Dumesnil, M. Dutheil, C. Dufour, and Ph. Mangin, Phys. Rev. B **62**, 1136 (2000).
[33] S. M. Watson, T. Hauet, J. A. Borchers, S. Mangin, and E. E. Fullerton, Appl. Phys. Lett. **92**, 202507 (2008).
[34] Z. J. Guo, J. S. Jiang, J. E. Pearson, S. D. Bader, and J. P. Liu, Appl. Phys. Lett. **81**, 2029 (2002).
[35] C. Ritter, J. Phys.: Condens. Matter **1**, 2765 (1989).
[36] E. E. Fullerton, J. S. Jiang, M. Grimsditch, C. H. Sowers, and S. D. Bader, Phys. Rev. B **58**, 12193 (1998).
[37] M. Sawicki, G. J. Bowden, P. A. J. de Groot, B. D. Rainford, J. M. L. Beaujour, R. C. C. Ward, and M. R. Wells, Phys. Rev. B **62**, 5817 (2000).
[38] F. Kneller and R. Hawig, IEEE Trans. Magn. **27**, 3588 (1991).
[39] O. Hellwig, J. B. Kortright, K. Takano, and E. E. Fullerton, Phys. Rev. B **62**, 11694 (2000).
[40] F. Radu, M. Etzkorn, R. Siebrecht, T. Schmitte, K. Westerholt, and H. Zabel, Phys. Rev. B **67**, 134409 (2003).
[41] R. Coehoorn, D. B. De Mooij, and C. De Waard, J. Magn. Magn. Mater. **80**, 101 (1989).
[42] L. H. Lewis, J. Kim, and K. Barmak, Physica B **327**, 190 (2003).
[43] H. Zeng, J. Li, J. P. Lu, Z. L. Wang, and S. Sun, Nature (London) **420**, 395 (2005).
[44] Y. Henry, S. Mangin, and F. Montaigne, Phys. Rev. B **69**, 140401(R) (2004).
[45] J. McCord, Y. Henry, T. Hauet, F. Montaigne, E. E. Fullerton, and S. Mangin, Phys. Rev. B **78**, 094417 (2008).
[46] J. S. Kouvel, Phys. Chem. Solids **16**, 152 (1960).
[47] K. Dumesnil, C. Dufour, Ph. Mangin, and A. Rogalev, Phys. Rev. B **65**, 094401 (2002).
[48] G. P. Felcher *et al.*, Rev. Sci. Instrum. **58**, 609 (1987).
[49] C. F. Majkrzak, Physica B **221**, 342 (1996).
[50] M. R. Fitzsimmons and C. F. Majkrzak, in *Modern Techniques for Characterizing Magnetic Materials*, edited by Y. Zhu (Kluwer, Boston, 2005), pp. 107–152.
[51] S. Park, M. R. Fitzsimmons, X. Y. Dong, B. D. Schultz, and C. J. Palmstrøm, Phys. Rev. B **70**, 104406 (2004).
[52] W. H. Press *et al.*, *Numerical Recipes: The Art of Scientific Computing* (Cambridge University Press, Cambridge, England, 1986), p. 294.
[53] I. K. Schuller, Phys. Rev. Lett. **44**, 1597 (1980).
[54] A. Hoffmann, S. G. E. teVelthuis, Z. Sefrioui, J. Santamaria, M. R. Fitzsimmons, S. Park, and M. Varela, Phys. Rev. B **72**, 140407(R) (2005).
[55] S. J. May, A. B. Shah, S. G. E. teVelthuis, M. R. Fitzsimmons, J. M. Zuo, X. Zhai, J. N. Eckstein, S. D. Bader, and A. Bhattacharya, Phys. Rev. B **77**, 174409 (2008).
[56] L. G. Parratt, Phys. Rev. **95**, 359 (1954).
[57] The difference between the magnetization of $YFe_2$ at 12 and 300 K is expected to be small since both temperatures are well below the Curie temperature (545 K) of $YFe_2$. See, L. Paolasini, R. Caciuffo, B. Roessli, G. H. Lander, K. Myers, and P. Canfield, Phys. Rev. B **59**, 6867 (1999).
[58] R. M. Richardson, J. R. P. Webster, and A. Zarbakhsh, J. Appl. Crystallogr. **30**, 943 (1997).
[59] C.-C. Lin, C.-H. Lai, R.-F. Jiang, and H.-P. D. Shieh, J. Appl. Phys. **93**, 6832 (2003).
[60] R. Morales, Z.-P. Li, J. Olamit, Kai Liu, J. M. Alameda, and Ivan K. Schuller, Phys. Rev. Lett. **102**, 097201 (2009).
[61] B. D. Cullity, *Introduction to Magnetic Materials* (Addison-Wesley, Reading, MA, 1972), p. 216.
[62] E. Goto, N. Hayashi, T. Miyashita, and K. Nakagawa, J. Appl. Phys. **36**, 2951 (1965).
[63] This implies the existence of anisotropy in a direction other than $[\bar{1}10]$. However, we found no dependence of the coercive field (obtained from vibration sample magnetometry) on the angle at which the field was applied parallel to the plane of a single-crystal $YFe_2$ thin film with respect to its in-plane crystallographic axes. Mössbauer spectroscopy of $YFe_2$ films in zero

field [A. Mougin, C. Dufour, K. Dumesnil, and Ph. Mangin, Phys. Rev. B **62**, 9517 (2000)] found the magnetization of single-crystal $YFe_2$ films to be aligned in a direction other than $[\bar{1}10]$.

[64] V. K. Vlasko-Vlasov, U. Welp, J. S. Jiang, D. J. Miller, G. W. Crabtree, and S. D. Bader, Phys. Rev. Lett. **86**, 4386 (2001).

[65] M. R. Fitzsimmons, P. Yashar, C. Leighton, Ivan K. Schuller, J. Nogués, C. F. Majkrzak, and J. A. Dura, Phys. Rev. Lett. **84**, 3986 (2000).

[66] To detect scattering from 10 nm lateral features requires access to $Q_{\parallel} > 0.01$ Å$^{-1}$. Because $Q_{\parallel}$ and $Q_{\perp}$ are coupled using the geometry of off-specular reflectometry, access to large $Q_{\parallel}$ means $Q_{\perp}$ is large, where even detection of the specular reflectivity challenges the limits of existing neutron reflectometers. Grazing incidence small-angle neutron scattering offers an opportunity to overcome the coupling between $Q_{\parallel}$ and $Q_{\perp}$, and this technique is being refined at several neutron-scattering facilities worldwide. See, for example, R. Pynn, M. R. Fitzsimmons, H. Fritzsche, M. Gierlings, J. Major, and A. Jason, Rev. Sci. Instrum. **76**, 053902 (2005).

[67] The optimum value for $K_{YFe_2}$ is reported. Acceptable values reported in Ref. 31 range from 0 to $5.7 \times 10^6$ erg/cm$^3$.

[68] C. Kittel and C. Herring, Phys. Rev. **77**, 725 (1950).